Letter Vol. 45, No. 2 / 15 January 2020 / Optics Letters 491

Broadband mid-infrared optical parametric oscillator for dynamic high-temperature multi-species measurements in reacting systems

Zachary E. Loparo,[1,2] Erik Ninnemann,[1] Qitian Ru,[2] Konstantin L. Vodopyanov,[2] and Subith S. Vasu[1,2,*]

[1]Center for Advanced Turbomachinery and Energy Research (CATER), Mechanical and Aerospace Engineering, University of Central Florida, Orlando, Florida 32816, USA
[2]CREOL, The College of Optics and Photonics, University of Central Florida, Orlando, Florida 32816, USA
*Corresponding author: subith@ucf.edu

Received 6 November 2019; revised 28 November 2019; accepted 10 December 2019; posted 16 December 2019 (Doc. ID 382308); published 10 January 2020

We demonstrate time-resolved simultaneous measurements of multiple hydrocarbons in high-temperature reacting and non-reacting mixtures using a broadband (instantaneous bandwidth 2.80–3.57 μm) subharmonic mid-infrared optical parametric oscillator based on orientation-patterned gallium phosphide. High-temperature absorption spectra and concentration time-histories of methane, ethane, and ethylene are measured at pressures around 2.3–2.7 atm and temperatures around 1235–1277 K in shock tube experiments.

https://doi.org/10.1364/OL.382308

The mid-infrared (MIR) spectral region is home to fundamental rovibrational absorption transitions of many combustion-relevant gas species, and is therefore a particularly useful spectral range for optical combustion diagnostics. MIR absorption spectroscopy for high-temperature reacting systems is well-established, but these techniques have largely employed narrowband fixed or swept/modulated lasers [1–3]. Spectrally broadband diagnostics with coherent laser beams provide richer information by probing the absorption spectrum over a large range rather than just a few lines or select features. Broadband measurements may be used to monitor multiple species, even with overlapping spectral features, as well as yield information on the temperature and pressure of the system.

Broadband radiation in the mid-infrared may be obtained using several types of sources. Benchtop blackbody sources produce broadband radiation spanning the MIR which is spatially incoherent, making them impractical for use over long path lengths. Supercontinuum lasers use intense pulses propagating through nonlinear waveguides to produce broad spectra [4], but require strong pump pulses to efficiently obtain output in the desired spectral range and are susceptible to optical damage. Subharmonic optical parametric oscillators (OPOs) can deliver a broadband spatially coherent output with spectral span over an octave, have low pump threshold due to doubly-resonant performance, and may be conveniently pumped by readily available 1.56 μm Er-fiber lasers [5,6].

Time-resolved spectroscopy at kHz rates has been used for combustion measurements in rapid compression machines based on both supercontinuum sources [7] and using dual-comb spectroscopy [8], but these measurements have been limited to the near-infrared (NIR) spectral region targeting overtone and combination bands. A MIR OPO based on a single frequency comb has been used to make time-resolved chemical kinetic measurements in a flowing cell reactor with repeating reaction events [9], but single mid infrared frequency combs have not been used to make fast time-resolved concentration measurements in non-repeating experiments. In this work, we use a mid-infrared frequency comb produced using a doubly resonant OPO as a spatially coherent broadband source to perform simultaneous multi-species measurements in high-temperature mixtures of shock-heated hydrocarbons.

Our broadband MIR diagnostic system used a subharmonic OPO which was based on the design detailed in Ref. [5] and is schematically sown in Fig. 1(a). Briefly, the OPO had a bowtie ring-type cavity, used a 0.5-mm-long orientation-patterned gallium phosphide (OP-GaP) nonlinear optical crystal, and was synchronously pumped by an Er-fiber mode-locked laser. The laser beam was coupled (mode matched) via a collimating lens into the OPO cavity through a dielectric incoupling mirror (M1). A CaF_2 wedge was used for OPO dispersion compensation and MIR beam outcoupling. Four additional flat gold mirrors (not shown) are used to fold the cavity and reduce the footprint, and the entire system was built on a 61 cm × 91 cm optical breadboard such that it could be moved and used in different experimental facilities. The OPO was encased in an acrylic purge box which was purged with dry N_2 to remove CO_2 and H_2O which introduce dispersion and limit the spectral output. Since the OPO operates in a doubly resonant (signal and idler) regime and had a very low pump threshold (41 mW of average power), we were able to use a miniature femtosecond mode-locked laser as a pump (Toptica FemtoFErb,

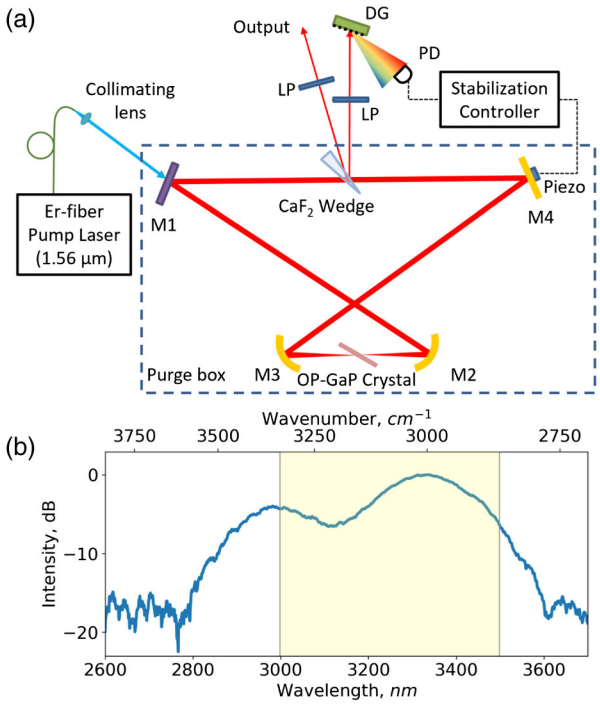

Fig. 1. (a) Schematic of the OPO. LP: long pass filter, DG: diffraction grating, PD: photodiode. M1 is a dielectric mirror transmissive to the pump and reflective for the OPO. M2 and M3 are gold-coated off-axis parabolic mirrors, and M4 is a piezo-mounted flat gold mirror. (b) Stabilized output spectrum of the OPO, log scale, with the highlighted region showing the range of the time-resolved spectrometer.

$\lambda = 1.56$ μm, 100 MHz, 50 fs, with 135 mW of max average power).

A doubly resonant OPO is interferometrically sensitive to cavity length detuning and operates at several resonant cavity lengths [5]. We have chosen the near-degenerate mode of operation, where the output extends from around 2800−3570 cm^{-1} (2.80–3.57 μm) with no gaps, as shown in Fig. 1(b). The spectral profile may also be fine-tuned by adjusting the thickness of the dispersion compensating wedge. The cavity length was actively stabilized to submicron accuracy via a piezo-mounted flat gold mirror (M4). One of two output MIR beams from the uncoated CaF_2 wedge was incident on a diffraction grating to disperse the spectrum. A mercury cadmium telluride (MCT) photodiode was placed such that it monitored the output intensity near a longwave edge of the broadband OPO spectrum, and its signal was used to stabilize the cavity length via side-of-fringe stabilization.

The transmitted spectrum of the OPO was measured during experiments using an in-house built time-resolved spectrometer (TRS), shown schematically in Fig. 2. The OPO output was coupled into the spectrometer via a $f = 35$ mm uncoated CaF_2 lens through an adjustable slit and collimated with a 2-in (5.08 cm) diameter, 200-mm focal length curved mirror. The collimated beam was incident on a 75 lines/mm diffraction grating, and the dispersed spectrum was focused by a second identical curved mirror onto the InSb detector array (30 μm pixel pitch) of a FLIR SC4000 IR camera. Calibration was performed by passing the OPO beam through a monochromator (Horiba iHR320) to obtain narrowband emission, with the

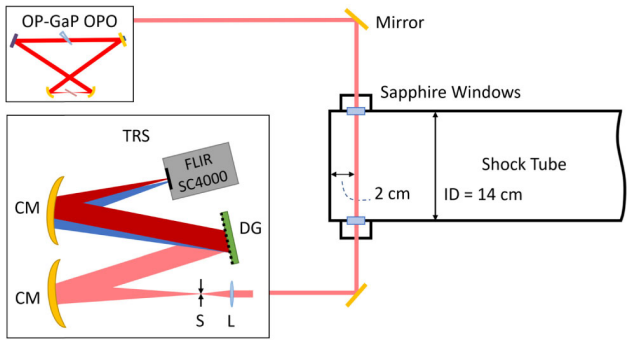

Fig. 2. Schematic of optical setup of the experiment and schematic of the TRS. L: CaF_2 lens, S: adjustable slit, CM: curved mirror, DG: diffraction grating.

output wavelength tuned over the range of the TRS. The wavelength was found to vary linearly with pixel position, and the instrument line shape was well modeled by a Gaussian profile with full-width at half-maximum of 6.8 nm. The spectral range accessed by the TRS was 2998–3498 nm, a range narrower than the output of the OPO highlighted region in Fig. 1(b), and was selected as a tradeoff between achieving broad spectral coverage and maintaining sufficient spectral resolution of the measurement due to the fixed number of camera pixels used, which was limited in order to achieve the desired time resolution for studying non-reproducible events. The range may be adjusted by rotating the grating to monitor different portions of the broadband MIR output of the OPO.

Our diagnostic system was used to perform multi-species measurements of mixtures of methane (CH_4), ethane (C_2H_6), and ethylene (C_2H_4) diluted in argon (Ar) in a 14-cm internal diameter shock tube, described in detail in previous work [10,11]. The mixtures studied in the experiments were 5% CH_4/95% Ar, 5%C_2H_4/95% Ar, 3%C_2H_6/97% Ar, and 1%CH_4/2%C_2H_4/97%Ar. Each mixture was filled into the tube and shock-heated to test conditions of pressures (P) of 2.3–2.7 atm and temperatures (T) of 1235–1277 K, with estimated uncertainties under 2% for both pressure and temperature [11]. The experimental setup is shown schematically in Fig. 2. The OPO beam was transmitted through the shock tube at the test location 2 cm from the endwall through a pair of wedged sapphire windows. Transmitted spectra were recorded at a frame rate of 21.477 kHz, the highest allowed for our 256 × 4 pixel window size, with an integration time of 37 μs. Data acquisition was triggered by the rise in pressure from the arrival of the reflected shock wave. The time-resolved absorbance spectra were based on measured spectra of the transmitted beam which were normalized to a reference spectrum taken before each experiment when the shock tube was evacuated.

First, we used the diagnostic system to measure high-temperature absorption spectra of CH_4, C_2H_4, and C_2H_6. Mixtures of the individual species diluted in argon were placed in the shock tube and shock-heated to temperatures around 1250 K and pressures around 2.5 atm, and their time-resolved absorption spectra were recorded. CH_4 and C_2H_4 don't break down at these conditions according to chemical simulations performed using the Aramco 3.0 chemical kinetic mechanism [12], so their absorption spectra were time-averaged over the first 2 ms of the experiment. C_2H_6 undergoes breakdown via pyrolysis at this temperature, so only the first absorption spectrum after

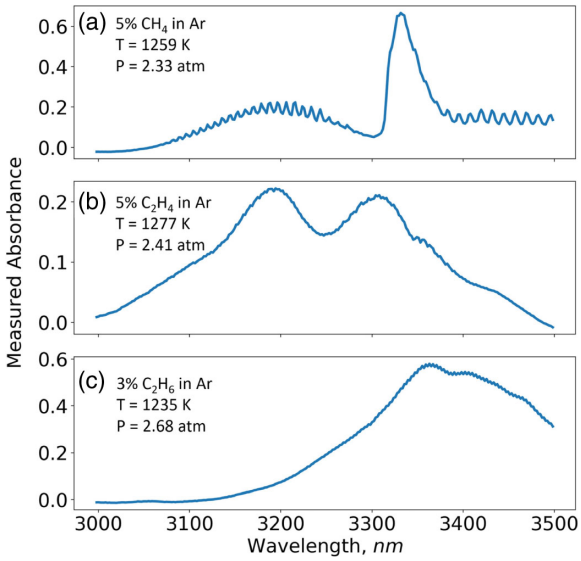

Fig. 3. Average measured absorbance spectra over the first 2 ms after the reflected shock for (a) CH_4 at 1259 K and 2.33 atm and (b) C_2H_4 at 1277 K and 2.41 atm. For (c) C_2H_6 at 1235 K and 2.68 atm, only the first spectrum after the reflected shock was used to measure the C_2H_6 absorbance spectrum before it began to break down via pyrolysis. The spectra are influenced by instrument broadening of the TRS.

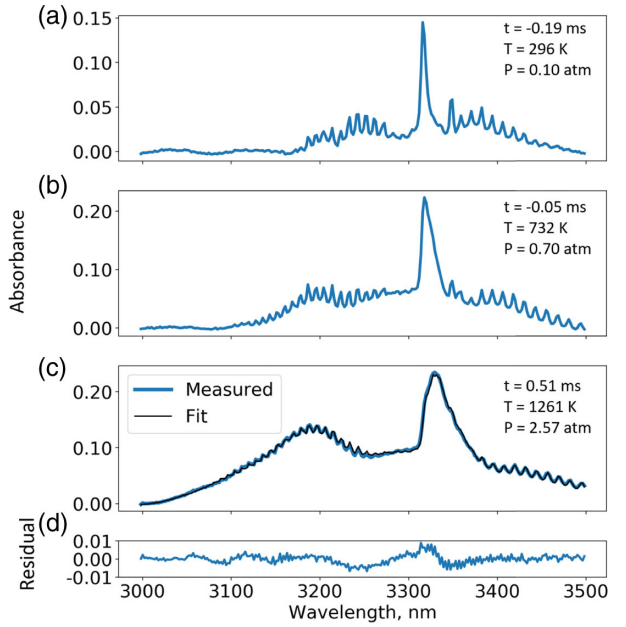

Fig. 4. Absorbance spectra of the $CH_4/C_2H_4/Ar$ mixture measured (a) before the incident shock wave at P = 0.10 atm, T = 296 K, (b) after the incident shock wave at P = 0.70 atm, T = 732 K, and (c) after the reflected shockwave at P = 2.57 atm and T = 1261 K, along with the fit, and (d) residual. Times are relative to the arrival of the reflected shockwave defining $t = 0$. Observed spectra are influenced by instrument broadening of the TRS.

the reflected shock wave is used. These reference absorption spectra, shown in Fig. 3, were used for calculating concentrations in multi-species measurement experiments, since spectral databases such as HITRAN 2016 [13] do not accurately model the studied hydrocarbons at the temperatures used in this study.

To determine species concentrations, measured absorption spectra from the experiment were analyzed using a least-squares fit of the reference spectra and characteristic baseline variations. During experiments, vibrations from the shock wave perturbed the OPO cavity length and caused the spectral output profile to change over time, resulting in a changing absorbance baseline. The characteristic changes in the OPO's spectral output profile due to vibrations were characterized by analyzing successive measured absorption spectra over a period of approximately 6 ms starting 40–60 ms after the reflected shock, where contribution to the absorption from the absorbing species was unchanging, thus isolating the change in spectral profile due to vibrations causing changes in the OPO cavity length. The principal components of the change in spectral profile were extracted via principal component analysis, and the first four principal components were used to fit the baseline, similarly to the description in Ref. [14].

Our MIR system was used to perform simultaneous concentration measurements in a non-reacting, high-temperature mixture by shock-heating the $1\%CH_4/2\%C_2H_4/97\%Ar$ mixture to T = 1261 K and P = 2.57 atm. At this temperature and pressure, no reaction or breakdown of the species in the mixture is expected to occur according to chemical kinetic simulations [12]. The measured absorbance spectra with baseline corrections are shown in Figs. 4(a)–4(c) for times before the incident shock, after the incident shock, and after the reflected shock. The different spectral features of the absorbing species are due primarily to the temperature-dependent changes in absorption profile and demonstrate the potential of the system to be used for thermometry. Measured and fit absorption spectra and residuals at time $t = 0.51$ ms after the reflected shock are shown in Figs. 4(c) and 4(d).

The measured and expected concentration time-histories of CH_4 and C_2H_4 are shown in Fig. 5(a). The observed concentrations are in good agreement with their expected values of 1% and 2%, and demonstrate the simultaneous species measurement capability of the system, even for species with completely overlapping absorption spectra.

The system was also used to simultaneously measure concentration time-histories of CH_4, C_2H_4, and C_2H_6 during the pyrolysis of a 3% C_2H_6 in a balanced Ar mixture at T = 1235 K and P = 2.68 atm. At these conditions, C_2H_6 undergoes pyrolysis and breaks down to form H_2, C_2H_4, CH_4, and several other minor species. Good agreement is seen between the measured concentrations and those predicted using the Aramco 3.0 chemical kinetic mechanism [12], and the trends for the depletion of C_2H_6 and formation of C_2H_4 and CH_4 are well captured, as shown in Fig. 5(b). Model uncertainty was estimated by performing the chemical kinetic simulation at temperatures 2% lower and higher than the test temperature of T = 1235 K, corresponding to the temperature uncertainty in the shock tube experiments. From 1.4–1.8 ms, the OPO output stopped due to vibrations from the shock, but resumed after stabilization was once again achieved.

Uncertainty in the measured concentrations is primarily due to the lack of instantaneous baseline reference spectra and the lack of temperature dependent reference absorption spectra for each species being measured. The estimated uncertainty shown accounts for the uncertainty in experimental temperature and pressure, fitting uncertainty via bootstrap error estimation, baseline spectrum fitting uncertainty by varying the number

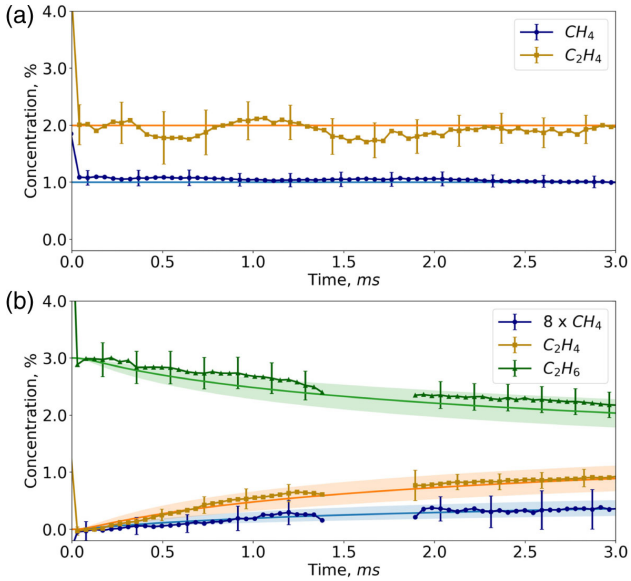

Fig. 5. Measured and expected time-histories for (a) the shock-heating of 1% CH_4 and 2% C_2H_4 in Ar to T = 1261 K and P = 2.57 atm, and (b) the pyrolysis of 3% C_2H_6 in Ar at T = 1235 K and P = 2.68 atm, with CH_4 scaled by 8× for visibility. Error bars indicate estimated uncertainty, and light bands in (b) indicate model uncertainty due to temperature for the C_2H_6 pyrolysis experiment.

of principal components used from 2–6, and uncertainty due to the measured reference absorption spectra by analyzing the reference experiments of Fig. 3 and measuring the deviation from the known concentrations. The reference absorption spectra shown in Fig. 3 do not have any baseline correction, but the characteristic changes in the OPO output spectrum were similar for all experiments so the baseline fitting procedure compensates for this. Obtaining time-resolved reference spectra during experiments and characterizing the absorption spectra for each species as a function of temperature will reduce uncertainty in future measurements.

The time and spectral resolution of the diagnostic system are limitations of the TRS. There is an inherent tradeoff between the framerate, spectral span, and spectral resolution using a dispersive spectrometer with a detector array readout, and these parameters should be adjusted to best suit the particular experiment. The time resolution of the system is a limitation of the framerate of the IR camera used, and could be improved by using a camera or linear detector array with a higher maximum framerate, or by reducing the number of pixels sampled at the expense of spectral information. The spectral resolution may be improved by reducing the spectral span or using more pixels at the cost of time-resolution.

Sensitivity of the OPO output spectrum to vibration may be reduced by improving the vibration isolation system and by tuning stabilization parameters, but is unlikely to be eliminated completely. In the future, a second portion of the camera will be used to record and occasionally read the reference spectrum during the experiment to reduce uncertainty, at a slight expense in overall measurement time resolution. The spectral coverage of this technique using single MIR OPOs may be extended with the appropriate detection hardware, to cover up to two octaves of spectral span [15] and address other functional groups, increasing the range of molecules the system can measure.

In conclusion, we demonstrate a diagnostic system based on a portable subharmonic MIR OPO operating around 2.8–3.6 μm for time-resolved concentration measurements of multiple hydrocarbons in high-temperature systems using a single line of sight. The system was used to obtain high-temperature absorption spectra of CH_4, C_2H_4, and C_2H_6, and measure their concentrations in both reacting and non-reacting experiments. The system can be applied to direct measurements of branching ratios and reaction rates for chemical kinetic model improvement, as well as for measuring absorption spectra of a range of combustion-relevant hydrocarbons at elevated temperatures and pressures to provide information relevant for improving spectral databases.

Funding. Defense Advanced Research Projects Agency (W31P4Q-15-1-0008); Office of Naval Research (N00014-15-1-2659); National Science Foundation (1144246).

Acknowledgment. Z. L. thanks the NSF for support under the Graduate Research Fellowship Program.

REFERENCES

1. C. S. Goldenstein, R. M. Spearrin, J. B. Jeffries, and R. K. Hanson, Prog. Energy Combust. Sci. **60**, 132 (2017).
2. Y. Ding, C. Strand, and R. Hanson, J. Quant. Spectrosc. Radiat. Transfer **224**, 396 (2019).
3. S. Wang, T. Parise, S. E. Johnson, D. F. Davidson, and R. K. Hanson, Combust. Flame **186**, 129 (2017).
4. C. R. Petersen, U. Møller, I. Kubat, B. Zhou, S. Dupont, J. Ramsay, T. Benson, S. Sujecki, N. Abdel-Moneim, Z. Tang, D. Furniss, A. Seddon, and O. Bang, Nat. Photonics **8**, 830 (2014).
5. Q. Ru, Z. E. Loparo, X. Zhang, S. Crystal, S. Vasu, P. G. Schunemann, and K. L. Vodopyanov, Opt. Lett. **43**, 21 (2018).
6. N. Leindecker, A. Marandi, R. L. Byer, and K. L. Vodopyanov, Opt. Express **19**, 6296 (2011).
7. T. Werblinski, P. Fendt, L. Zigan, and S. Will, Appl. Opt. **56**, 4443 (2017).
8. A. D. Draper, R. K. Cole, A. S. Makowiecki, J. Mohr, A. Zdanowicz, A. Marchese, N. Hoghooghi, and G. B. Rieker, Opt. Express **27**, 10814 (2019).
9. A. J. Fleisher, B. J. Bjork, T. Q. Bui, K. C. Cossel, M. Okumura, and J. Ye, J. Phys. Chem. Lett. **5**, 2241 (2014).
10. Z. E. Loparo, J. G. Lopez, S. Neupane, W. P. Partridge, K. Vodopyanov, and S. S. Vasu, Combust. Flame **185**, 220 (2017).
11. Z. E. Loparo, E. Ninnemann, K. Thurmond, A. Laich, A. Azim, A. Lyakh, and S. S. Vasu, Opt. Lett. **44**, 1435 (2019).
12. C.-W. Zhou, Y. Li, U. Burke, C. Banyon, K. P. Somers, S. Ding, S. Khan, J. W. Hargis, T. Sikes, O. Mathieu, E. L. Petersen, M. A. AlAbbad, A. Farooq, Y. Pan, Y. Zhang, Z. Huang, J. Lopez, Z. Loparo, S. S. Vasu, and H. J. Curran, Combust. Flame **197**, 423 (2018).
13. I. E. Gordon, L. S. Rothman, C. Hill, R. V. Kochanov, Y. Tan, P. F. Bernath, M. Birk, V. Boudon, A. Campargue, K. V. Chance, B. J. Drouin, J.-M. Flaud, R. R. Gamache, J. T. Hodges, D. Jacquemart, V. I. Perevalov, A. Perrin, K. P. Shine, M.-A. H. Smith, J. Tennyson, G. C. Toon, H. Tran, G. Tyuterev, A. Barbe, G. Császár, M. Devi, T. Furtenbacher, J. Harrison, J. Hartmann, A. Jolly, J. Johnson, T. Karman, I. Kleiner, A. A. Kyuberis, J. Loos, M. Lyulin, S. Massie, S. Mikhailenko, N. Moazzen-Ahmadi, S. Muller, O. V. Naumenko, A. V. Nikitin, O. L. Polyansky, M. Rey, M. Rotger, S. Sharpe, K. Sung, E. Starikova, S. Tashkun, J. Auwera, G. Wagner, J. Wilzewski, P. Wcisło, S. Yu, and E. J. Zak, J. Quant. Spectrosc. Radiat. Transfer **203**, 3 (2017).
14. M. C. Phillips, M. S. Taubman, B. E. Bernacki, B. D. Cannon, R. D. Stahl, J. T. Schiffern, and T. L. Myers, Analyst **139**, 2047 (2014).
15. V. Smolski, H. Yang, S. Gorelov, P. G. Schunemann, and K. L. Vodopyanov, Opt. Lett. **41**, 1388 (2016).